Geodinamica Acta

Publication details, including instructions for authors and subscription information:
http://www.tandfonline.com/loi/tgda20

Paleozoic magmatic events in the Strandja Massif, NW Turkey

Gürsel Sunal [a b], Boris A. Natal'in [a], Muharrem Satir [b] & Erkan Toraman [c d]

[a] Istanbul Technical University, Department of Geology , TR-34390 , Istanbul , Turkey

[b] Universität Tübingen, Institut für Geowissenschaften , Wilhelmstrasse 56, D-72074 , Tübingen , Germany

[c] Department of Earth and Atmospheric Sciences , Saint Louis University , 329 Macelwane Hall 3507 Laclede Ave., St. Louis , MO , 63103 , USA

[d] ITU Eurasia Institute of Earth Sciences , TR-34390 , Istanbul , Turkey

Published online: 13 Apr 2012.

To cite this article: Gürsel Sunal , Boris A. Natal'in , Muharrem Satir & Erkan Toraman (2006) Paleozoic magmatic events in the Strandja Massif, NW Turkey, Geodinamica Acta, 19:5, 283-300, DOI: 10.3166/ga.19.283-300

To link to this article: http://dx.doi.org/10.3166/ga.19.283-300

Geodinamica Acta

Geodinamica Acta 19/5 (2006) 283-300

Paleozoic magmatic events in the Strandja Massif, NW Turkey

Gürsel Sunal [a,b,*], Boris A. Natal'in [a], Muharrem Satır [b], Erkan Toraman [c, d]

[a]* *Istanbul Technical University, Department of Geology, TR-34390 Istanbul, Turkey*

[b] *Universität Tübingen, Institut für Geowissenschaften, Wilhelmstrasse 56, D-72074 Tübingen, Germany*

[c] *Department of Earth and Atmospheric Sciences, Saint Louis University, 329 Macelwane Hall 3507 Laclede Ave. St. Louis, MO 63103 USA*

[d] *ITU Eurasia Institute of Earth Sciences, TR-34390 Istanbul, Turkey*

Received: 31/03/05, accepted: 09/03/06

Abstract

The Strandja massif consists of metamorphic basement intruded by large Early Permian plutons of the Kırklareli type and overlain by Triassic metasedimentary cover. Together with its continuation in Bulgaria this massif forms an important link between the Pontides and the orogenic belts of Europe. Various types of orthogneisses constitute a significant part of the metamorphic basement however these rocks have until now escaped a particular study and therefore the Paleozoic history of the massif is essentially unknown. In this study these rocks are classified and mapped as hornblende-biotite, biotite-muscovite, and leucocratic orthogneisses. Their modal compositions correspond to quartz diorite, tonalite, granodiorite and trondhjemite. Geochemical data suggest a calc-alkaline trend of differentiation and metaluminous character of the parent magmas. Isotopic dating using the single zircon evaporation method has shown that magmatic ages of these orthogneisses cluster within a short time interval between 312±2 and 315 ±5 Ma in the Carboniferous. At the same time inherited ages of magmatic zircons in these rocks record a long lived magmatic activity between 340 and 650 Ma. We infer that the Carboniferous orthogneisses were formed in a magmatic arc that evolved atop of a mature continental basement. Previously established ([1, 2]) Early Permian magmatic event has been confirmed by additional age determinations constraining it at 257±6 Ma. Tectonic setting of this episode is also interpreted as subduction related taking into consideration its geochemical features and relationships with surrounding tectonic units.

Keywords: Carboniferous granitoids/ Strandja Massif/ single zircon Pb/Pb evaporation ages

1. Introduction

The Strandja massif occupies the northern half of the Thrace province of northwestern Turkey and neighboring regions of Bulgaria (Fig. 1b). In Bulgaria, its continuation is known as a Balkan terrane consisting of Paleozoic rocks [3-5). In Turkey, the Strandja massif is interpreted as a part of the Pontides [6] that is an orogenic belt consisting of fragments of the Cimmerian microcontinent of Gondwanian origin, which collided with Eurasia during the early Mesozoic Cimmerian orogeny [7]. This interpretation of the Pontides is still shared by many researches while others infer that the Strandja massif along with the Istanbul zone belonged to the Laurasian margin during the Late Paleozoic and Mesozoic [8, 9].

Summaries on geology of the massif have been provided by [1, 2, 10-12]. According to these studies the Strandja massif consists of the metamorphosed basement that is intruded by granites and unconformably overlain by the Triassic to Jurassic metasedimentary cover. Timing of tectonic events was constrained by the following isotopic age determina-

* Corresponding author.
Tel: +90 212 2856162 – Fax +90 212 2856210
E-mail address: gsunal@itu.edu.tr

tions. Aydın [1] reported 244±11 Ma Rb-Sr whole-rock age for the Kırklareli metagranites that intrude the basement. Using zircon evaporation method Okay *et al*. [2] dated the same granites as well as the Kula pluton located to the north as 271±2 Ma old (mean of 5 and 2 grains respectively). The Üskup metagranites that are exposed to the east of the Kırklareli pluton yielded 309±24 Ma (ages obtained from a single grain). Zircons from country rock gneisses yielded somewhat younger ages – 266±14, 239±16 Ma (single grain), and 278±19 Ma (single grain). A single zircon from migmatites associated with the metagranites yielded four different ages 299±15, 276±12, 239±12, and 221±14 Ma. Two last age determinations have been considered as unreliable because of the inferred Triassic age of the sedimentary cover (Okay *et al*., 2001). The Kırklareli granites also yielded biotite K-Ar ages of 150-149 Ma, Rb-Sr biotite whole-rocks age of 144 Ma [1, 10], and Rb-Sr biotite and whole-rock age of 155±2 Ma [2]. All of these ages were interpreted as the age of regional metamorphism.

This limited database explains why the Paleozoic tectonic history of the Strandja massif was never discussed in detail. Concerning the Permian magmatism, Şengör *et al*. [13] interpret it as subduction-related paired with a south-dipping subduction zone while Okay *et al*. [2] consider it as collisional.

Various gneisses and schists metamorphosed in amphibolite facies have been described in the Paleozoic basement [1, 12]. Interpretations of their ages vary from the Precambrian [11, 14] to "late Variscan" [2]. A significant part of these rocks is represented by orthogneisses some which were interpreted as metamorphic equivalents of the early Permian granites [12]. Our geological mapping and structural studies have shown that the main part of the so-called Teke Dere group that unites all country rocks of the early Permian granites [12] consists of orthogneisses suggesting a long magmatic history of the Strandja massif in a magmatic arc tectonic setting [15].

The goal of this study is to present new data on geochronology and petrology of orthogneisses constituting a significant portion of the Paleozoic basement of the Strandja massif. Using zircon evaporation method and conventional U-Pb method we have established a prolonged history of the Paleozoic magmatic activity with peaks at 314.7±2.6, 312.3 ±1.7, and 257 ± 6.2 Ma. Inherited zircons in orthogneisses suggest an additional magmatic episode around 350 Ma. These data allow a better correlation of the tectonic activity of the Strandja massif with surrounding regions and newly obtained geochemical data impose constraints on tectonic settings of the massif in the Paleozoic.

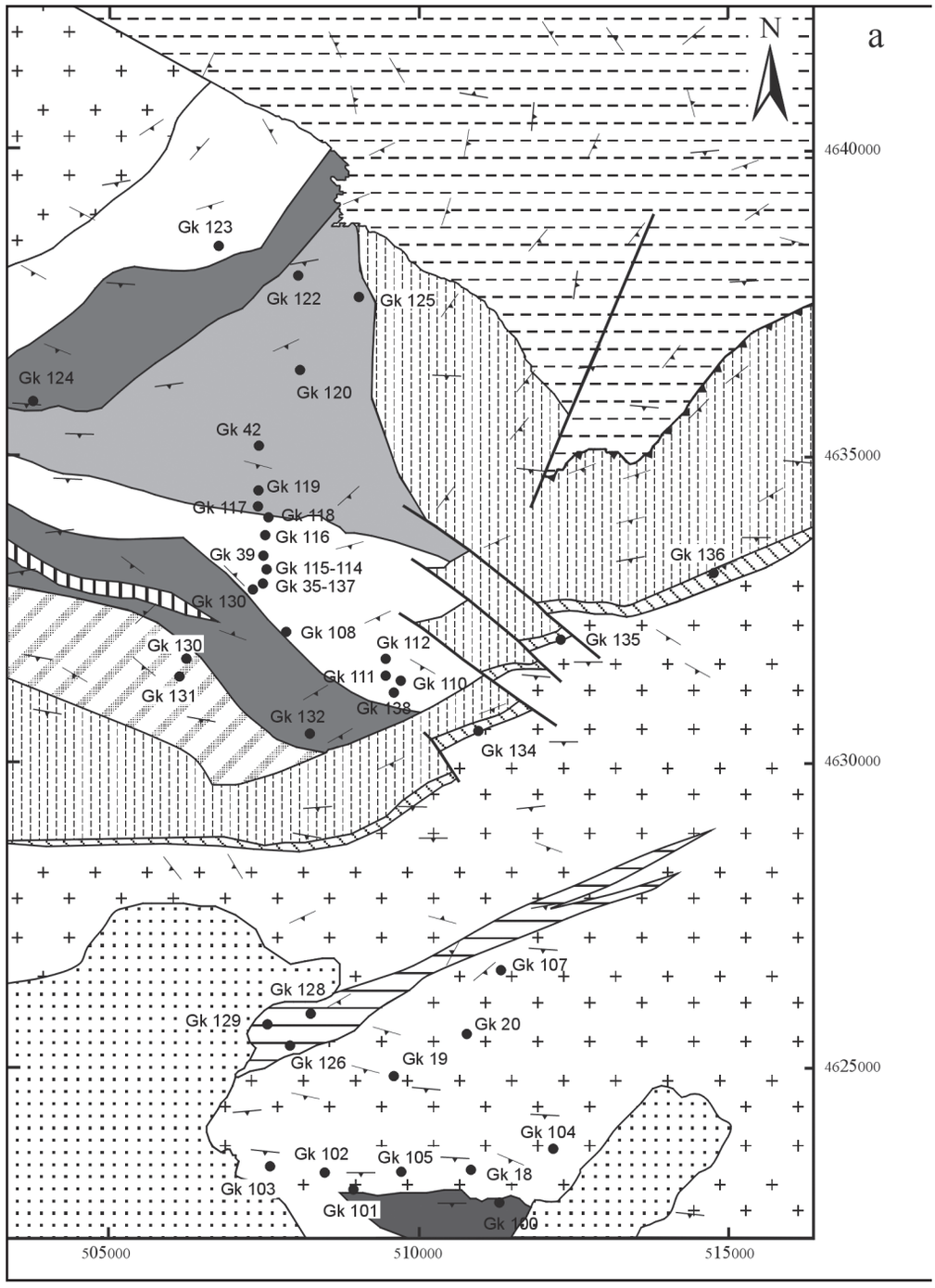

2. Tectonic units of the studied area

Similar to previous studies we recognized in the studied area the Paleozoic basement, early Permian Kırklareli granites, and overlying them the Triassic metasedimentary cover. The

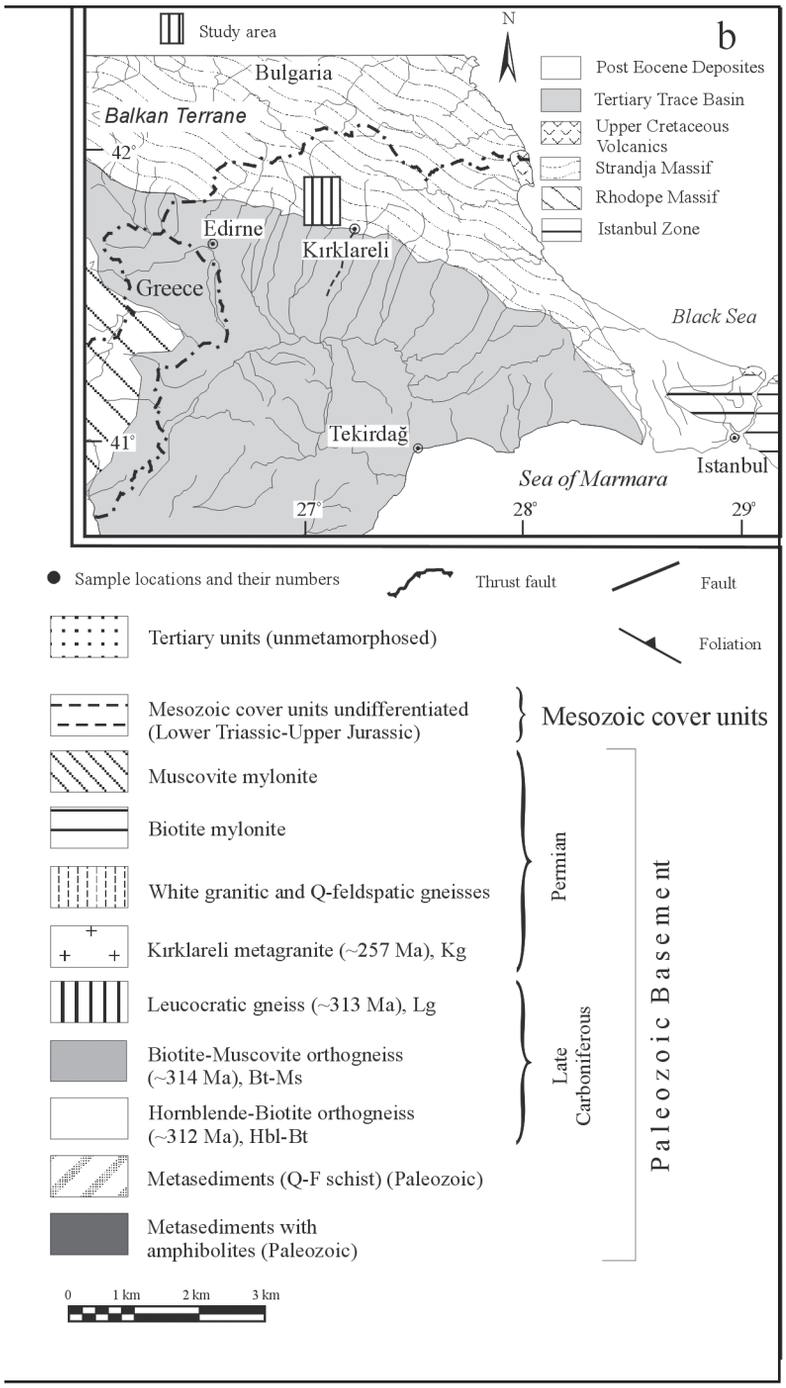

Figure 1:
a- Simplified geological map of the study area (after Natal'in *et al*. [16]), **b**- Map shows main tectonic divisions and the position of the Strandja Massif in Marmara region.

basement consists of biotite-muscovite paragneisses, biotite schists, amphibolites, and several types of orthogneisses three of which were formed before the emplacement of the Kırklareli granites (Fig. 1a, [16]). These rocks strike northwest and have consistent moderate dips to the southwest. The Kırklareli granites form a large (25x14 km) pluton slightly elongated in the east-west direction. Along its margins, the granites are converted to mylonitic gneisses. The Triassic metasedimentary cover starts with metaconglomerates containing clasts of granite gneisses, quartzites, quartz, and schists. They grade up into quartz-rich metasandstones containing lens-shape bodies of metaconglomerates and diamictites. These rocks are metamorphosed in greenschist facies. Clasts in metaconglomerates and diamictites have their own foliation indicating an episode of metamorphism and deformation preceding the accumulation of the massif cover. The age of cover rocks is inferred from long-distance correlations with Bulgarian part of the Strandja massif [12, 2] where Triassic fossils have been found in rocks of a similar lithology [3, 17].

Original relationships between tectonic units are almost completely obliterated by the late Mesozoic deformations and metamorphism that occurred between late Jurassic and early Cretaceous (136-171 Ma) (Natal'in *et al*., in preparation). The late Mesozoic deformation and metamorphism formed penetrative foliation that in many places strikes at a high angle to lithological boundaries. It reworked earlier formed fabric and mineral assemblages hindering the reconstruction of the Paleozoic-early Mesozoic history of the Strandja massif.

In following sections we give a description of the orthogneisses in the basement and Kırklareli granite. Information on other rock units and structural history of the region will be published elsewhere (Natal'in *et al*., in preparation).

2.1. Hornblende- biotite orthogneisses

The hornblende-biotite orthogneisses constitute two elongated bodies in the western part of the studied area (Fig. 1a). Generally, these rocks reveal strong foliation and mineral lineation, but in places they are massive and preserve their original magmatic fabric. The orthogneisses are medium grained rocks, greenish gray to gray in color. They consist of quartz (10-25 %), albite-oligoclase (35-40 %), biotite (5-15 %), hornblende-actinolite (5-10 %), epidote (15-20 %), chlorite (3-5 %), and muscovite (5 %) with ratio between light and dark minerals similar to granite-granodiorite. Mafic dykes and schlierens of amphibolite are common feature of these rocks. Composition of amphibolites varies from dioritic to gabbroic (Hbl-Bt schlieren in Table 1 and Fig. 2). Amphibole is bluish-green in color; plagioclase is strongly decomposed. The schlierens vary in shape form equidemensional to strongly elongate. The elongated schlierens occurring in weakly foliated and lineated rocks suggest their origin because of magma flow [18, 19]. The schlierens and mafic dykes may be interpreted as evidence of magma mixing during the formation of the parent granitoids [20, 19]. In places, xenoliths of biotite schists similar to country rocks were observed.

2.2. Biotite-muscovite orthogneisses

The biotite-muscovite orthogneisses form a large body in the northern part of the mapped area (Fig. 1a). Similar to the hornblende-biotite orthogneisses they are represented by

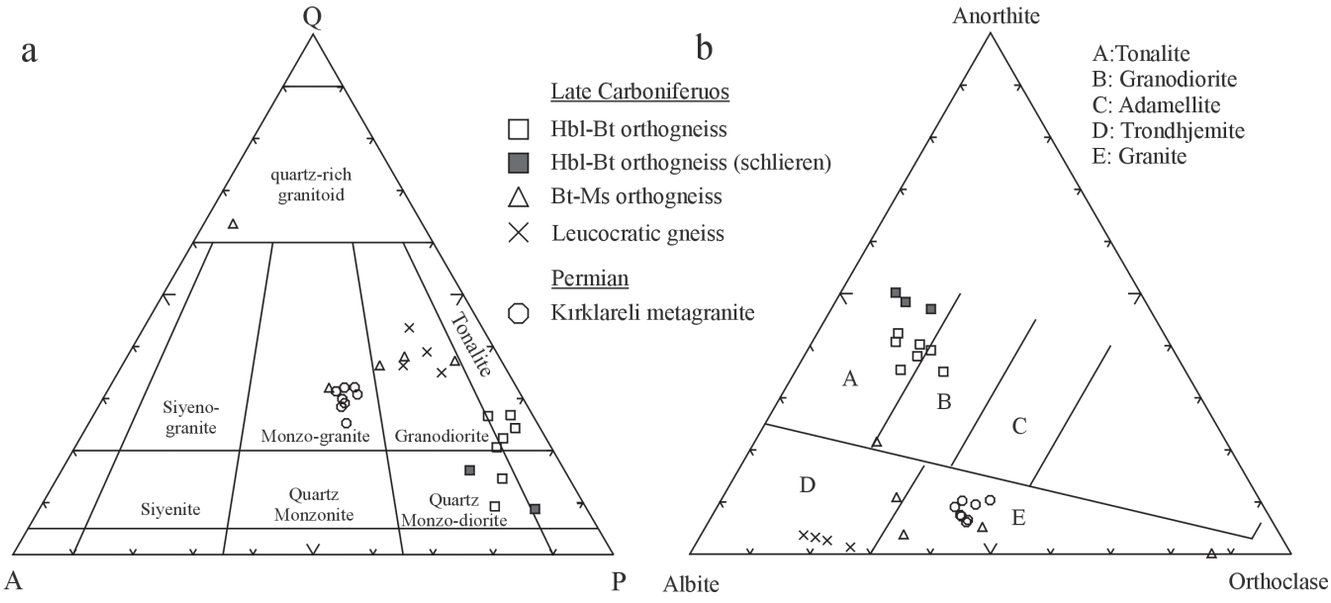

Figure 2:
Plot of normative compositions of the orthogneisses and granitoids in **a**- quartz-alkalifeldspar-plagioclase (Q-A-P) diagram (LeMaitre [28]), **b**- The normative anorthite-albite-orthoclase compositions of the units (O'Connor [29]). Hbl-Bt: hornblende-biotite; Bt-Ms: biotite-muscovite.

foliated and weakly foliated or unfoliated rocks. The later preserve good evidence for magmatic origin of rocks. The weakly to unfoliated granite constitute lens shape bodies that vary from ten meter to 500 m across.

The biotite-muscovite granite gneisses are medium grained, greenish-gray to gray in color. Their mineral composition is similar to the hornblende-biotite orthogneisses except the absence of hornblende and a greater content of muscovite (5-10 %). Weakly strained rocks are very homogenous while foliated rocks sometimes reveal a vague compositional layering. In contrast to the hornblende-biotite granite gneisses schlierens and biotite xenoliths are absent in the biotite-muscovite granite gneisses.

2.3. Leucocratic orthogneisses and granites

The hornblende-biotite and biotite-muscovite orthogneisses as well as surrounding metasedimentary rocks are cut by dykes of leucocratic granite gneisses and granites. Thickness of these dykes varies from several centimeters to several tens meters. A closely spaced swarm of this rock is shown in Fig. 1a. In places the leucocratic granitic rocks are strongly foliated and folded. At the same time some bodies are not foliated at all though they cut foliated granite gneisses. These rocks are enigmatic because foliation in granite gneisses is Mesozoic in age. Presence of metamorphic muscovite in the leucocratic rocks suggest that these rocks somehow were affected by metamorphism but resisted deformation. Leucocratic orthogneisses consist of quartz (35-45 %), plagioclase (35-45 %), K-feldspar (15-25 %), muscovite (10-15 %), chlorite (2-4 %), biotite (<1 %), and opaque minerals (1-2 %).

The leucocratic granites and granite gneisses are mainly exposed within the medial Paleozoic gneisses and among Paleozoic metasediments to the south of the Kırklareli granites. They are absent within the Kırklareli pluton.

2.4. Kırklareli metagranites

The Kırklareli monzogranites constitute a large pluton located to the north of Kırklareli (Fig. 1b). Geological structure of its western part is shown on the map (Fig. 1a). The Kırklareli monzogranites consist of quartz (25-30 %), plagioclase (13-20 %), K-feldspar (35-47 %), biotite (5-10 %), muscovite (2-4 %), epidote, chlorite and others (1-2 %). The characteristic feature of these rocks is porphyric fabric with large (4 cm) pink crystals of K-feldspar. These crystals make the magmatic origin of rocks obvious however the granites usually reveal clear metamorphic foliation dipping to the south at moderate angles. Quartz always has undulose extinction and often recrystallized into fine-grained aggregates. Plagioclase is strongly altered. K-feldspar is often characterized by microcline twining and marginal replacement by myrmekites. Biotite is brown to dark green in color. Kinking and bending of its crystal, grains shredding along cleavage planes, displaced cleavage fragments of former grains that form wedge shape terminations are very common for biotites in thin sections. Some times biotite forms typical folia wrapping around K-feldspar. All of these structural features indicate solid state deformation of the Kırklareli granites in accord with criteria described by Vernon [20]. Muscovite replaces the biotite and we disagree with a previously published conclusion on its magmatic origin [2].

Migmatites are widespread along the southern margin of the Kırklareli pluton. There, intrusive contacts of the granites and country rocks were also observed. In the north and northwest the Kırklareli granites are framed by

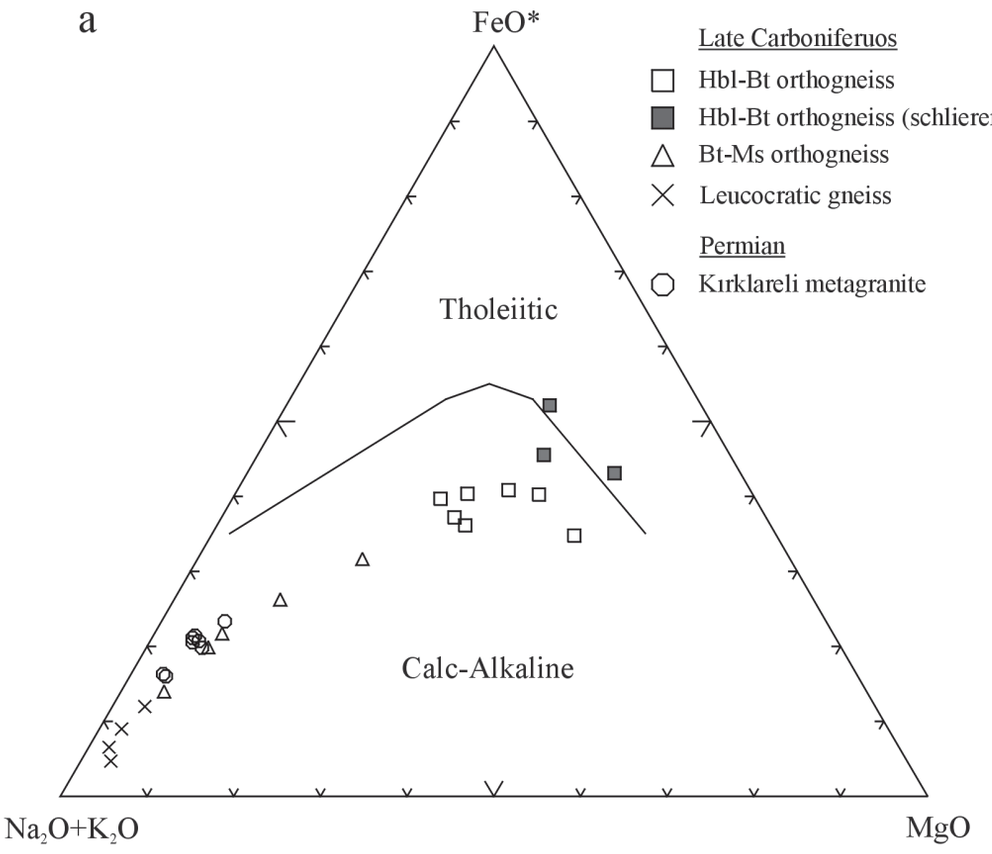

Figure 3:
a- Tholeiitic-calc-alkaline description of the Irvine and Baragar [69]. Note that all of orthogneisses follow a single trend on the AFM diagram being within the calc-alkaline field. Abbreviations are the same as in figure 2.

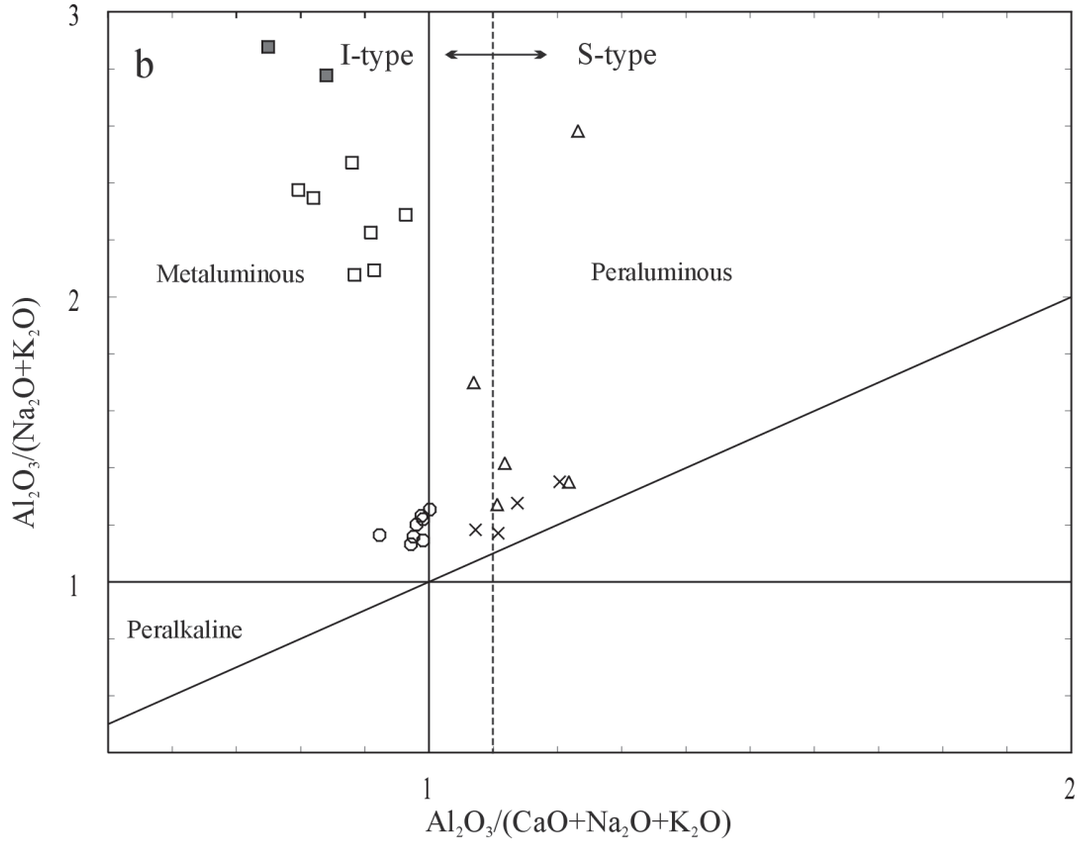

b- Plot of the Shand's index for granitoids in the study area. Discrimination fields for different types of granitoids (Maniar and Piccoli [67], Shand [68]) are shown.

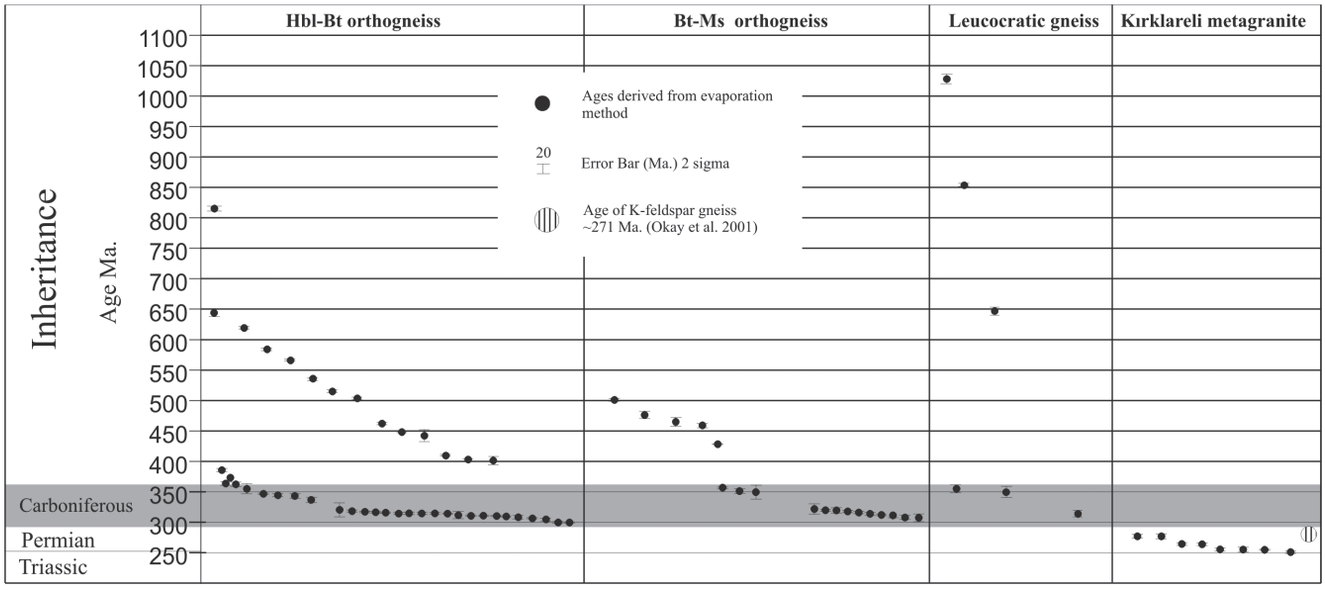

Figure 4: Summary chart of the ages of the units derived from single grain evaporation method. Ages older than 1.3 Ga. are not plotted in this diagram. Errors bars represent two-sigma standard deviations (2σ). Abbreviations are the same as in figure 2.

mylonitic granite gneisses (Fig. 1a). These fine- to medium-grained rocks are very homogeneous in composition and often contain floating porphyroblasts of pink K-feldspar as well as lower strained lenses of porphyric granites similar to the Kırklareli type. We interpret them as a part of the pluton affected by ductile shearing.

3. Two episodes of magmatic activity

All orthogneisses and Kırklareli metagranites reveal penetrative foliation that has consistent attitude (Fig. 1a). This foliation has Mesozoic age as it is evident from available isotopic dating [1, 10, 2]. In places, the hornblende-biotite and biotite-muscovite granite gneisses preserve two foliations made of biotite. There is only one foliation in the Kırklareli granites. The earlier foliation indicates an episode of metamorphism and deformation separating emplacement of the will be added hornblende- and biotite-muscovite orthogneisses and the intrusion of the Kırklareli granites. The absence of leucocratic granite gneisses in the Kırklareli pluton suggests that they were formed together with the hornblende-biotite and biotite-muscovite orthogneisses. Geological relationships have been confirmed by isotopic dating indicating the Carboniferous age of the hornblende-biotite, the biotite-muscovite and the leucocratic orthogneisses (see below) and the Permian age of the Kırklareli granite (our data and data presented by Aydın [10] and Okay *et al*. [2]). These two groups of rocks are distinct in terms of their geochemical signature.

4. Analytical techniques

The whole-rock powders were split from 1-5 kg of crushed rocks. Major and trace elements were determined by x-ray fluorescence spectrometry at the University of Tübingen, Germany. For this study rock powders was mixed with $Li_2B_2O_7$ (1.5:7.5) and then were fused at 1150ºC into glass discs. Total iron is expressed as Fe_2O_3. Loss of ignition (LOI) was calculated after heating the sample powder to 1000ºC for 1 hour.

Zircons were extracted from rock samples by standard mineral separation techniques, Wilfley table, heavy liquids, Frantz isodynamic separator and were finally handpicked under a binocular microscope. Then a fraction with grain sizes 63-200 μm was classified according to crystal properties (i.e. euhedral morphology, lack of overgrowth and visible inclusions). For cathodoluminescence (CL) studies, zircons were mounted in epoxy resin and polished down to expose grain interiors. CL images were obtained by Technocyn 8200 Mk 4 Luminascope fitted with an Alcatel Vacuum Pump. The chamber is mounted on a Zeiss Microscope which has had the normal stage replaced by CL chamber.

For single-zircon Pb-evaporation, chemically untreated, grains were analyzed using a double Re filament configuration suggested by Kober [21, 22]. Note that a group of zircons used for the evaporation is not the same that was used for CL studies. We simply rely of identity of these two groups in our interpretations of ages. Each zircon was embedded in a Re evaporation filament and placed in front of a 1 mm wide Re ionization filament. Then it was heated first at 1350 °C for 5-10 min for removal of common and radiogenic Pb hosted in less stable phases (e.g. in crystal domains affected by radiation damage), which have low activation energies [21]. During repeated evaporation-deposition cycles in 20 °C steps Pb is deposited to ionization filament for the measurements starting at about 1380 °C. Only high counts, generally 20.000-200.000 per second for ^{206}Pb were used for age evaluations. Pb isotopes

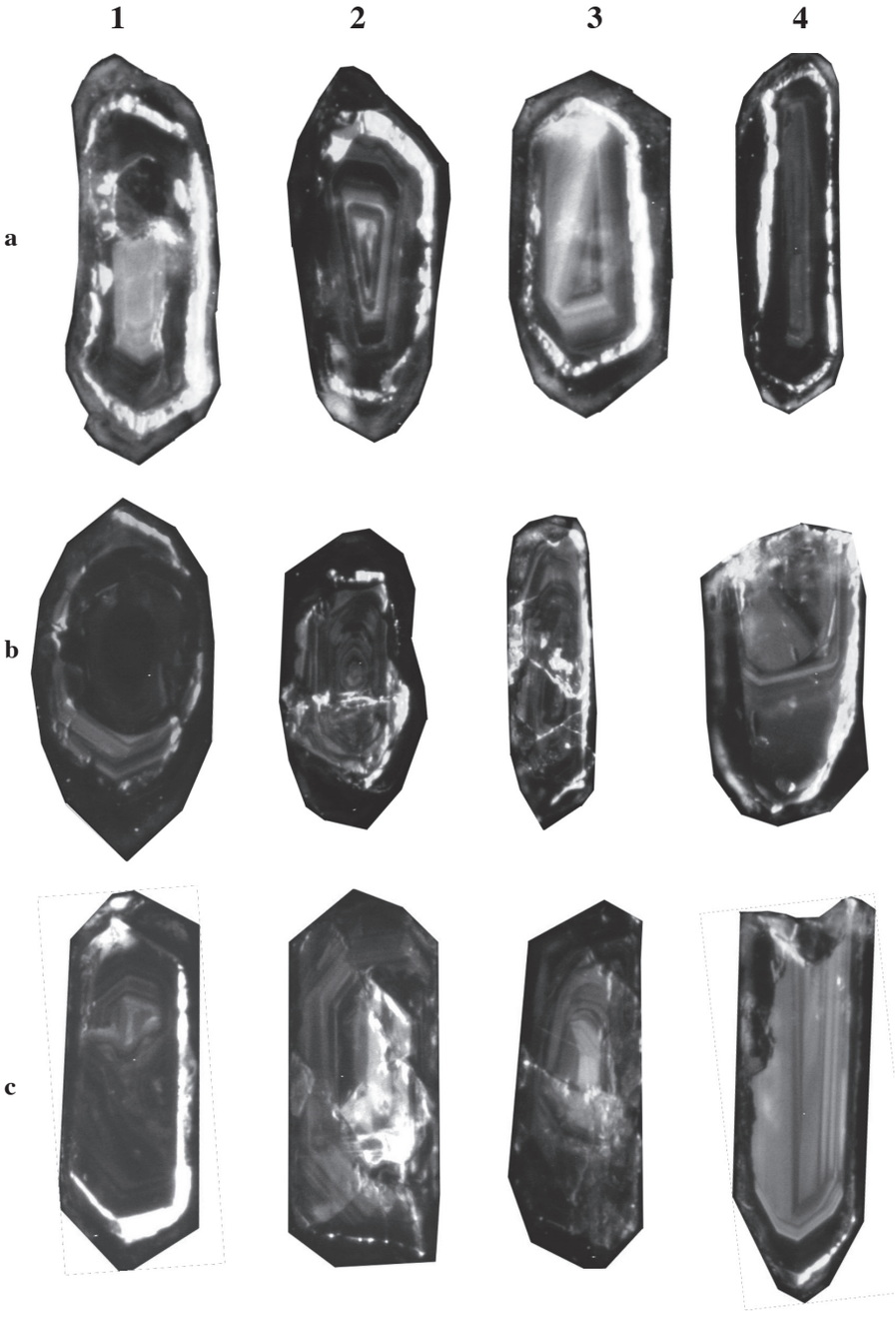

Figure 5: CL images of selected grains of;
a- biotite-muscovite orthogneiss,
b- hornblende-biotite orthogneiss,
c- Kırklareli metagranite. All of the grains show oscillatory magmatic zoning.
Figures 1a and 1b have core structures (for discussion see text).

were dynamically measured in a sequence of 206-207-208-204-206-207 with a secondary electron multiplier. Correction of the common lead contribution to measured $^{207}Pb/^{206}Pb$ ratios is made in accord with the two-stage growth model of Stacey and Kramers [23]. Further detailed information on method is given in Chen *et al*. [24], Okay *et al*. [2], and Siebel *et al*. [25]. All isotopic ratios were measured in static mode on a Finnigan-MAT 262 multicollector mass spectrometer at the Tübingen University, Germany.

The $^{207}Pb/^{206}Pb$ ages are based on the means of all measurements evaluated and the errors are given by the 2σ (2 sigma) standard deviation. The age and error for several grains from the same sample are given as weighted mean and error of the weighted mean, respectively. $^{207}Pb/^{206}Pb$ evaporation ages during the course of measurements for Redwitzites granites yielded an average age of 322.8 ± 4.1 Ma, similar to those age ranges reported by Siebel [26] and Siebel [25].

For conventional U–Pb analysis, non-magnetic zircon populations consisting of morphologically identical grains were washed in hot 6N HCl and hot 7N HNO_3 prior to remove surface contamination. Further detailed information on method is given in Chen *et al*. [24], Siebel *et al*. [25], and Nguyen [27].

5. Results

5.1. Major and trace element geochemistry

5.1.1. Carboniferous magmatism

Chemical composition of the hornblende-biotite and biotite-muscovite granite gneisses is shown in (Table 1). Modal compositions the hornblende-biotite granite gneisses fall in the tonalites and quartz monzodiorite fields when plotted on quartz – alkali-feldspar – plagioclase (QAP) diagram (Fig. 2a, [28]). Compositions of the biotite-muscovite and leucocratic orthogneisses form a cluster within the granodiorite field (Fig.2a). On the anorthite – albite – orthoclase (AAO) diagram [29] the hornblende-biotite orthogneisses are within the tonalite and granodiorite fields (Fig. 2b). The biotite-muscovite orthogneisses are scattered in the granite, trondhjemite, and granodiorite fields while leucocratic orthogneisses fall in the trondhjemite field (Fig. 2b).

The hornblende-biotite gneisses contain about 50-60 wt. % SiO_2 and 14-19 wt. % Al_2O_3. Low content of SiO_2 was obtained from schlierens. The biotite-muscovite orthogneisses are more felsic in composition. Their SiO_2 content in the biotite-muscovite gneisses range between 66-76 wt. % and they have relatively low Al_2O_3 contents of 14-15 wt. %. The leucocratic gneiss reveal yet higher SiO_2 contents (76-80 wt. %) and further decrease of the Al_2O_3 contents between 12 and 15 wt. %.

Table 1. Major and trace element compositions of the units. Hbl-Bt: hornblende-biotite; Bt-Ms: biotite-muscovite.

	Bt-Ms orthogneiss					Hbl-Bt orthogneiss							Hbl-Bt schlieren		
Sample	Gk117	Gk119	Gk120	Gk122	Gk125	Gk108	Gk111	Gk115	Gk116	Gk118	Gk35	Gk123	Gk114	Gk137	Gk138
SiO_2	72.937	73.375	69.134	76.541	72.601	59.217	56.935	58.035	55.801	53.686	59.941	60.67	50.559	53.527	51.028
TiO_2	0.242	0.39	0.579	0.159	0.481	0.764	0.691	0.856	0.838	1.293	0.747	0.73	1.081	0.981	0.798
Al_2O_3	14.799	14.889	15.055	14.374	14.182	16.501	15.618	17.493	16.545	18.927	17.302	17.409	18.072	15.455	14.755
$Fe_2O_3^{tot}$	1.7	2.396	4.363	1.83	3.372	7.397	7.759	7.555	8.615	7.63	6.356	6.559	10.836	12.089	10.769
MnO	0.034	0.03	0.055	0.014	0.042	0.137	0.145	0.115	0.151	0.127	0.09	0.102	0.182	0.218	0.381
MgO	0.547	0.775	2.356	0.592	1.414	5.099	8.407	4.511	6.758	4.95	3.488	4.675	7.071	6.333	9.52
CaO	0.957	0.665	2.871	0.167	1.474	6.642	6.821	6.254	7.594	6.772	5.705	5.9	8.25	8.392	10.26
Na_2O	3.641	4.36	3.996	0.484	4.11	3.111	2.82	3.329	3.247	3.44	3.05	3.697	2.72	2.528	2.429
K_2O	5.219	3.555	2.111	4.852	2.998	1.441	1.859	2.204	1.502	3.188	2.352	2.062	1.878	1.121	0.829
P_2O_5	0.21	0.167	0.166	0.131	0.12	0.209	0.141	0.198	0.177	0.579	0.198	0.169	0.185	0.191	0.169
LOI	1.36	1.56	2.14	0.95	1.91	1.1	1.06	0.98	1.02	1.31	0.75	0.97	1.41	1.11	0.89
Ba	548.2	789.8	525.7	416.2	786.8	622.3	509.7	587.4	379.5	706.6	668.1	608.1	520.3	547.5	228
Co	86.6	85.3	96.7	82.4	85.9	90.7	89.4	87.7	86.7	65	19.4	92.8	95.2	73	78.3
Cr	9.2	12.7	45.6	8	32.1	208.6	643	168.9	361.2	74.9	109	219.7	160.1	287.2	528
Ni	na.	na.	1.8	na.	na.	32.9	121	17.7	34.7	19.8	27.8	32	18.7	37.7	67.8
Rb	170.8	139.1	91.1	151.8	100.4	52	79.9	90.6	54.3	129.4	88.7	78.1	90.2	33.1	28.5
Sr	182.3	149.7	260.8	23.9	205.8	461.8	271.8	298.9	303.8	603.4	513.4	306.6	459.6	303.3	191.9
V	15.7	31.8	72.5	10.9	65.6	140.3	157.4	134.4	165.6	183.6	117	111.9	263.7	228.3	230.9
Y	20.2	26.3	40.7	22.9	45.8	24.5	24.7	27.8	24.8	33.5	22.6	21.9	45.3	53.3	45.4
Zn	7.6	12.2	3.9	na.	9.4	78.7	79.6	73	82.5	83.7	84.9	58.2	112.4	144.6	192.3
Zr	147.5	222.1	197.1	113.1	194.6	141.4	108	152.9	98.5	141.2	157.4	146.8	117.5	90.6	77.9
Ce	58.2	98.9	80.1	na.	81.2	57.1	49.1	47.9	53.9	103.4	46.6	na.	85	82.8	71.6
Eu	0.6	0.9	1	na.	0.9	1.5	0.9	1.1	1.1	1.8	1.5	1	1.7	1.7	1.2
La	34.8	44.1	48.6	10.6	42.3	41.9	29.6	27.8	32.3	51.6	52.4	20.1	45.9	39.3	34.7
Nb	8.6	9.5	na.	na.	11.6	na.	na.	na.	na.	21.1	na.	na.	17.3	20.7	21.2
Nd	25.3	42.3	40.8	8.3	34.3	25	22.2	27.3	26.3	49.9	28	22.3	39.3	48.1	29.2
Pb	45.5	18.1	22	4.8	14.4	10.4	17.8	14	13.7	14.9	21.1	15.5	16	9.1	28.5
Sm	5.2	8.5	6	na.	6	4.9	3.3	4.8	4.2	6.9	5.5	3.1	7.4	9.8	5.4
Th	19.9	27	16.3	5.6	26	2.4	8.4	4.6	3.8	9	2.8	3.6	na.	0	5.1
U	na.	na.	na.	na.	na.	na.	na.	na.	na.	na.	2.2	na.	na.	na.	na.
Yb	1.6	2	3.5	2.1	4.1	2.1	2.1	2.4	2.1	3.1	2	1.8	4.3	5.1	4.4
Total	101.79	102.33	102.98	100.18	102.88	101.82	102.48	101.71	102.42	102.13	100.17	103.12	102.45	99.93	102.02
#Mg	0.39	0.39	0.51	0.39	0.45	0.57	0.68	0.54	0.61	0.56	0.52	0.58	0.56	0.51	0.63
#ASI	1.11	1.22	1.07	2.26	1.12	0.88	0.82	0.91	0.80	0.88	0.96	0.91	0.84	0.75	0.63

Table 1. continue

	Kırklareli metagranite								leucocratic gneiss			
Sample	Gk18	Gk100	Gk102	Gk103	Gk104	Gk105	Gk107	Gk124	Gk101	Gk110	Gk112	Gk113
SiO_2	71.482	70.138	73.032	70.575	72.93	73.934	74.133	70.363	77.88	80.418	77.107	76.272
TiO_2	0.424	0.475	0.282	0.415	0.36	0.378	0.26	0.535	0.08	0.078	0.055	0.093
Al_2O_3	13.872	14.227	13.728	13.989	13.71	14.012	13.326	13.369	13.843	12.337	15.079	14.661
$Fe_2O_3^{tot}$	2.653	2.831	2.013	2.807	2.555	2.758	1.958	3.222	0.655	0.406	0.886	1.152
MnO	0.049	0.044	0.05	0.05	0.057	0.056	0.045	0.061	0.011	0.008	0.043	0.037
MgO	0.649	0.824	0.471	0.568	0.562	0.553	0.398	0.905	0.21	0.267	0.232	0.327
CaO	1.537	1.14	1.028	1.455	1.513	1.443	1.181	1.649	0.363	0.581	0.785	0.723
Na_2O	3.37	4.15	3.942	3.681	3.742	4.015	3.87	3.871	5.294	4.942	5.909	5.289
K_2O	5.098	5.305	5.085	5.005	4.593	4.681	4.751	4.727	2.879	2.13	1.935	1.993
P_2O_5	0.123	0.146	0.089	0.12	0.1	0.113	0.082	0.194	0.147	0.226	0.233	0.261
LOI	0.32	0.65	0.33	0.31	0.31	0.31	0.29	1.67	0.67	0.6	0.58	0.99
Ba	628.7	842.8	391.6	620	416.4	392.3	300	642.6	79.3	454	137.3	293.4
Co	5	100.7	96.3	131.7	139.1	103.2	136.1	93.8	91.3	105.9	1.6	0.5
Cr	4.3	8.9	8.7	8	7.7	7.3	7.4	7.5	4.9	5.9	7.9	6.7
Ni	na.	na.	na.	na.	na.	na.	na.	na.	na.	na.	na.	na.
Rb	197.2	143.4	222.4	196.9	214.7	215.8	235.8	154.7	108.7	65.1	60.2	65.3
Sr	123.9	101.8	78.7	116.4	92	87.5	63.8	112.6	47	130.9	103.6	84.1
V	30.5	33.7	17.8	26.2	26.5	29.6	18.9	33.4	3.2	7.1	1.2	3.7
Y	30.6	36.4	32.4	35.3	33.9	35.9	36.4	33.2	14.6	8.9	8.2	15.4
Zn	43.3	3.6	11.6	7.8	7.6	22.2	na.	18.1	na.	na.	na.	9.6
Zr	211.1	228.9	176.4	208	168.1	203.9	156.6	204.5	90.4	110.2	91.9	105.5
Ce	83.8	124.5	61.1	78	77.6	91.4	68.1	113.4	na.	na.	na.	na.
Eu	0.7	0.8	0.4	0.6	0.5	0.6	0.3	0.7	0.2	0.4	0.4	0.4
La	62.4	52.5	33.2	35.3	37.7	41.9	39.5	52.2	18.1	na.	14.1	12.3
Nb	10.6	na.	12.9	13.9	11.9	13.9	14.7	11.3	9.1	na.	9.1	8.7
Nd	44.8	52.9	33.8	43.2	36	44.4	32.6	53.5	10.8	5	3	4.3
Pb	24	10.3	29.7	28.8	31.6	32.5	32.5	16.7	8.4	27	6	14.5
Sm	7.2	9.2	4.7	5.7	5.7	7.1	5.1	7.4	2.7	2.2	2.5	3.3
Th	19.8	20	17.8	22.4	17.6	29.1	24.4	22.5	5.5	7.5	1.2	6.2
U	na.	na.	na.	na.	na.	na.	na.	na.	na.	1.5	1.8	na.
Yb	2.7	2.9	2.9	3	3	3.1	3.3	2.7	1.3	0.6	0.5	1.2
Total	99.73	100.11	100.17	99.13	100.57	102.39	100.41	100.72	102.08	102.09	102.89	101.86
#Mg	0.32	0.36	0.31	0.28	0.30	0.28	0.29	0.36	0.39	0.56	0.34	0.36
#ASI	1.00	0.97	0.99	0.99	0.99	0.98	0.98	0.92	1.11	1.07	1.14	1.20

$Fe_2O_3^{tot}$: represent the total iron amount, #Mg: $[MgO/(Fe_2O_3^{tot} *0.9+MgO)]$, ASI = molecular $Al_2O_3/(CaO+Na_2O+K_2O)$, na. : not determined

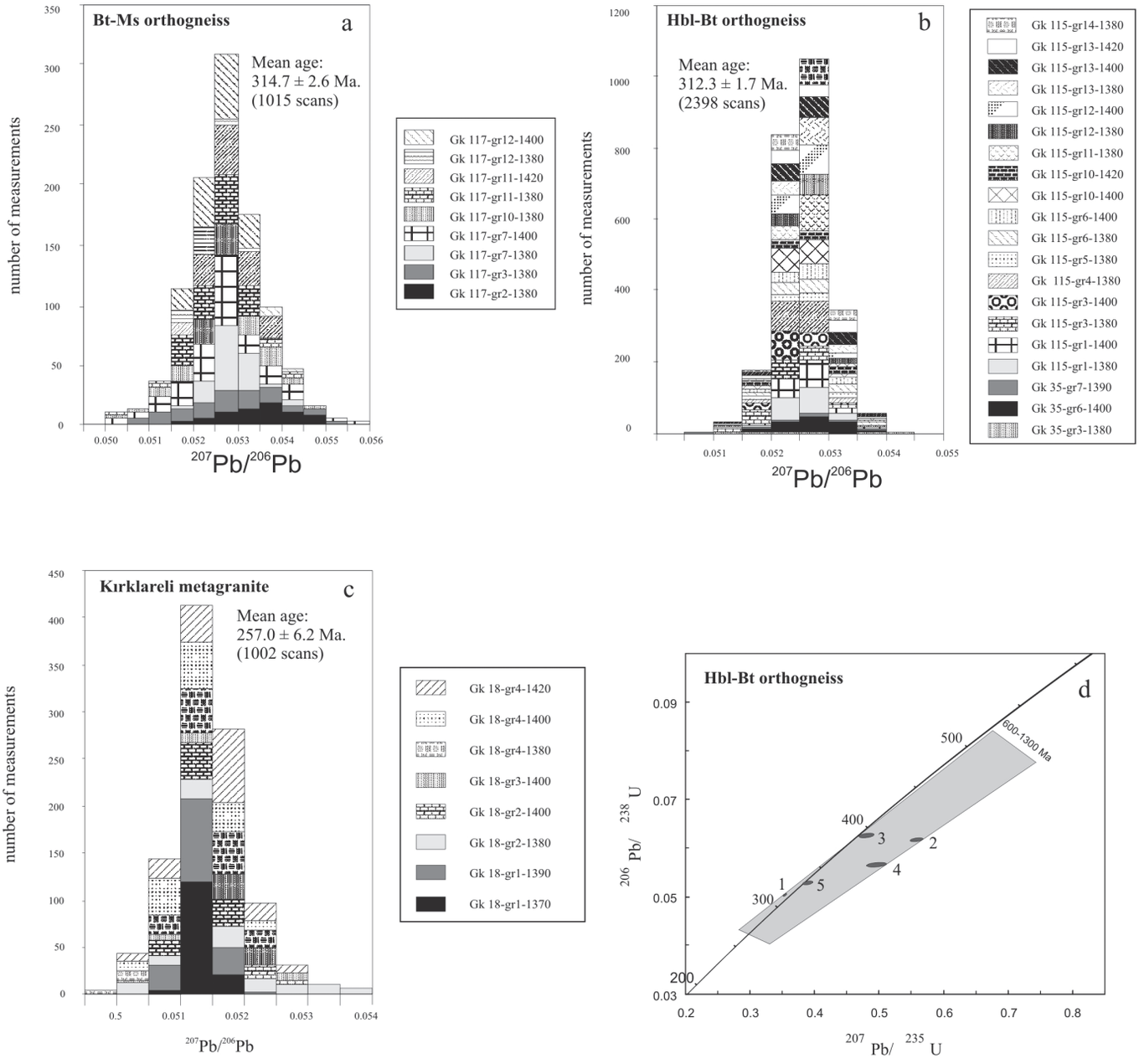

Figure 6: Histograms showing the frequency distributions of radiogenic $^{207}Pb/^{206}Pb$ ratios derived from evaporation of single zircon grains:
a- biotite-muscovite orthogneiss,
b- hornblende-biotite orthogneiss,
c- Kırklareli metagranite.
d- U–Pb concordia plots for zircon analyses of the hornblende-biotite orthogneiss (Gk 35). The upper intercept ages are calculated from zircon fractions taking a forced regression through 310 Ma. Ellipses indicate 2σ errors. The data were calculated with ISOPLOT program (Ludwig [70]). Abbreviations are the same as in figure 2.

XMgO [MgO/(Fe_2O_3 ^{tot} *0.9+MgO)] values vary between 0.51 and 0.68 in the hornblende-biotite gneisses, and between 0.39 and 0.51 in the biotite-muscovite gneiss (Table 1). The aluminum saturation index [ASI = molecular $Al_2O_3/(CaO+Na_2O+K_2O)$] ranges from 0.63 to 0.91 in the hornblende-biotite gneisses, and from 1.07 to 2.26 in the biotite-muscovite gneisses (Fig. 3b and Table 1). XMgO [MgO/(Fe_2O_3 ^{tot} *0.9+MgO)] values of the leucocratic gneisses vary between 0.33 and 0.56, and ASI values between 1.1 and 1.2 (Fig. 3b and Table 1). Note that all three types of orthogneisses follow a single trend on the AFM diagram being within the calc-alcalkaline field (Fig. 3a)

5.1.2. Permian magmatism

In a ternary Quartz-Alkalifeldspar- Plagioclase (Q-A-P) diagram (Fig. 2a, [28]), the Kırklareli K-feldspar metagranites form a tight group within the monzogranite field. On the normative anorthite– albite–orthoclase diagram [29] they are

Table 2. Age of biotite-muscovite orthogneisses derived from single grain evaporation method. Errors are two-sigma standard deviations (2σ).

Sample/Grain	Evaporation temp. C	No. of scans	Mean ratio of $^{207}Pb/^{206}Pb$/error	Age (Ma)	Error (Ma)±
Gk117					
grain1	1400	110	0.05620 ±18	460.3	7.1
grain1	1420	177	0.05652 ±18	472.9	6.9
grain2	1380	66	0.05352 ±19	350.9	7.9
grain3	1380	110	0.05277 ±21	318.9	9.1
grain3	1400	180	0.05372 ±14	359.3	5.9
grain4	1380	146	0.055397 ±41	428.3	1.7
grain4	1400	36	0.05627 ±54	463	21
grain6	1400	148	0.053645 ±80	356.2	3.2
grain6	1420	144	0.05725 ±11	501.2	4.4
grain7	1380	145	0.05251 ±16	307.7	7.1
grain7	1400	105	0.052782 ±82	319.4	3.6
grain10	1380	74	0.05259 ±19	311.2	8.4
grain10	1400	37	0.05283 ±41	321.5	17
grain11	1380	33	0.05249 ±30	306.8	13
grain11	1400	111	0.05264 ±14	313.3	5
grain11	1420	108	0.052733 ±82	317.3	3.6
grain12	1380	145	0.052604 ±64	311.8	2.7
grain12	1400	147	0.052681 ±85	315.5	3.6
grain13	1380	34	0.05348 ±55	349.2	23

in the granite field (Fig. 2b). Comparing with the previously described rock types the Kırklareli metagranites have a more restricted content of SiO_2 – 70-74 wt. % and Al_2O_3 – 13-15 wt. % (Table 1). Their XMgO [MgO/(Fe_2O_3 ^{tot} *0.9+MgO)] values vary between 0.28 and 0.36 (Table 1) and ASI values between 0.9-1 (Fig. 3b and Table 1). Similar to hornblende-biotite, biotite-muscovite, and leucocratic orthogneisses the K-feldspar metagranites shows calc-alkaline affinity, occurring on the trend defined for the older magmatic complexes (Fig. 3a).

5.2 Geochronology

Figure 4 shows the general distribution of ages obtained by single grain evaporation method in the Strandja Massif. Scattered and inherited ages are also indicated in this diagram.

5.2.1. Carboniferous granitoids

5.2.1.1. Biotite-muscovite gneiss

Only one sample Gk117 has been used for isotopic age determinations of these rocks (see Fig. 1 for location). All zircons extracted from this sample have prismatic partly corroded crystals with 1:2 and 1:3 aspect ratios (Fig. 5a). Their cathodoluminescence (CL) images show magmatic oscillatory zoning indicating a magmatic origin (Fig. 5a). Three distinct populations have been recognized: 1) dark brown, semi-transparent; 2) colorless to light brown, transparent; and 3) greenish, semi-transparent. The only grain of the first population yields 460±7 and 472±7 Ma ages (grain 1 in Table 2). The second population has mixed ages varying from 319±9 to 463±21 Ma (grains 2, 3, 4, 13 in Table 2) increasing with an increase of the evaporation temperature. Greenish and semi-transparent crystals yield ages of 307±13 and 319±4 Ma (grains 7, 10, 11, 12 in Table 2). The Cl images of zircons do not exhibit any inherited core except grain 1a in Fig. 5 that shows a dark body which is difficult to interpret. However old ages especially those obtained with the increase of evaporation temperature suggest the presence of inherited core in the analyzed zircons.

Consistent ages of greenish zircons reflect the magmatic ages of the biotite-muscovite orthogneisses. It has a weighted average mean of 314.7 ± 2.6 Ma (mean of 6 grains and 9 heating steps, Table 2, Fig. 6a). In all of the zircon images a high CL zone is surrounded by low CL on the outer side which is parallel with oscillatory zoning in the inner parts of crystals. Both of these zones may indicate a metamorphic overprint [30] and thus explain a scatter of magmatic ages between 309 and 319 Ma.

Table 3. Ages of hornblende-biotite orthogneisses derived from single grain evaporation method. Errors are two-sigma standard deviations (2σ).

Sample/Grain	Evaporation temp. C	No. of scans	Mean ratio of $^{207}Pb/^{206}Pb$/error	Age (Ma)	Error (Ma)±
Gk35					
grain1	1380	72	0.05378 ±19	361.9	7.9
grain2	1380	36	0.05333 ±18	342.9	7.7
grain2	1420	249	0.05761 ±11	515	4.2
grain2	1440	36	0.06626 ±34	814.6	11
grain3	1380	36	0.05280 ±54	320.2	23
grain3	1400	143	0.054751 ±81	402.5	3.4
grain3	1420	109	0.05626 ±12	462.6	4.7
grain4	1420	107	0.055750 ±47	442.4	19
grain5	1400	37	0.05361 ±42	354.7	17
grain5	1450	70	0.05382 ±15	363.5	6.1
grain6	1400	107	0.052756 ±78	318.3	3.4
grain7	1390	37	0.05260 ±28	311.6	12
grain7	1430	37	0.05473 ±34	401.2	14
grain8	1400	36	0.06113 ±36	643.8	13
grain9	1400	74	0.05317±23	336.1	9.1
Gk115					
gr1	1380	145	0.052581 ±53	310.8	2.3
gr1	1400	148	0.052573 ±47	310.4	2
gr3	1380	144	0.052327 ±82	299.7	3.6
gr3	1400	146	0.052324 ±43	299.6	1.8
gr4	1380	184	0.052544 ±42	309.2	1.8
gr5	1380	74	0.05252 ±14	308.1	6.1
gr6	1380	111	0.052668 ±86	314.5	3.6
gr6	1400	109	0.052667 ±90	314.5	3.9
gr7	1450	141	0.058991 ±68	566.8	2.6
gr8	1380	109	0.13429 ±28	2154.8	3.7
gr8	1400	72	0.16275 ±17	2484.4	1.7
gr9	1420	107	0.05946 ±13	584.0	4.8
gr9	1450	109	0.11581 ±22	1892.5	3.4
gr10	1400	145	0.052483 ±45	306.5	2.0
gr10	1420	73	0.05243 ±11	304.2	4.6
gr11	1380	146	0.052661 ±33	314.2	1.4
gr11	1400	73	0.05336 ±11	344.1	4.8
gr11	1420	36	0.05435 ±13	385.6	5.4
gr12	1380	108	0.052694 ±61	315.7	2.7
gr12	1400	146	0.052569 ±40	310.2	1.8
gr13	1380	142	0.052722 ± 52	316.9	2.3
gr13	1400	145	0.052668 ±66	314.5	3.0
gr13	1420	108	0.052668 ±90	314.5	3.9
gr14	1380	144	0.052708 ±52	316.3	2.3
gr14	1400	145	0.053413 ±65	346.4	2.7
gr14	1420	112	0.05731 ±11	503.5	4.2
gr16	1400	74	0.058136 ±97	534.9	3.7
gr16	1420	103	0.06044 ±14	619.4	4.7

Table 4. U–Pb zircon analytical data of hornblende-biotite orthogneisses (sample Gk 35). All errors are two-sigma standard deviations (2σ). Measured U–Pb data were calculated ISOPLOT program (Ludwig, 2003) using 2 σ errors. See text for discussion.

Sample	$^{206}Pb^*/^{204}Pb$	U (ppm)	Pb* (ppm)	$^{208}Pb^*/^{206}Pb^*$	$^{206}Pb^*/^{238}U$	$^{207}Pb^*/^{235}U$	$^{207}Pb^*/^{206}Pb^*$	Apparent ages (Ma) $^{206}Pb^*/^{238}U$	$^{207}Pb^*/^{235}U$	$^{207}Pb^*/^{206}Pb^*$
Hb-Bt gneiss										
Gk35-1	9212	334	16.7	0.15	0.05021±27	0.3554±27	0.05134±27	308.8	315.8	256.2
Gk35-2	4230	444	27.3	0.10	0.06152±78	0.5589±30	0.06589±79	450.8	384.9	802.9
Gk35-3	484	329	20.4	0.18	0.06234±96	0.4817±40	0.05603±66	399.2	389.8	453.9
Gk35-4	119180	249	13.8	0.08	0.05640±120	0.4970±38	0.06391±153	409.7	353.7	738.6
Gk35-5	2681	364	19.2	0.12	0.05267±58	0.39076±28	0.05380±75	334.9	330.9	362.7

5.2.1.2. Hornblende- biotite gneiss

Two samples (Gk115 and Gk35) of the hornblende-biotite gneisses have been dated using single-zircon $^{207}Pb/^{206}Pb$ step-wise-evaporation method (see Fig. 1 for location). All zircons in these samples are idiomorphic and prismatic. They are classified into two groups: 1) colorless or light brown, transparent and translucent (Fig. 5 b-1 and 2), and 2) dark brown, semi-transparent, euhedral prismatic grains (Fig. b-3 and 4). Cathodoluminescence images show that all grains exhibit oscillatory magmatic zoning testifying the magmatic origin of the zircons. A presence of inherited rounded core in the grain b1 (Fig. 5b1) suggests that some zircons contain older cores incorporated during the formation and emplacement of the hornblende-biotite granites. Note that the inherited core also has the oscillatory magmatic zoning. All of the grains exhibit low CL outer rims representing a metamorphic overprint.

Six grains in the sample Gk115 gave young ages between 300 and 320 Ma at all evaporation steps. All of these grains belong to the first morphological group. Grains 11 and 14 of the same group revealed increasing of ages with increase of the evaporation temperature. Grains 3 and 7 (first group) of the sample Gk35 have similar behavior. The increase of ages in these grains reflects the presence of inherited cores. Old dates in these grains are difficult to interpret because they may indicate ages of inherited cores or mixed ages of the cores and young magmatic overgrowth. Zircons of the second group (grains 8, 9 and 16 in the sample Gk115 and grains 3 and 7 in sample Gk35) yielded ages older than 340 Ma at all heating steps (Table 3). These zircons represent xenocrysts incorporated by granitic magma from older intrusions.

Fig. 6b shows a histogram of $^{206}Pb/^{207}Pb$ ratios obtained from both samples and plotted on the same diagram. Note that peaks of the sample Gk 115 and Gk 35 fit each other giving age of 312.3 ±1.7 Ma (weighted mean of 13 grains, 20 heating steps). We accept this date as the magmatic age of the hornblende-biotite orthogneisses.

Beside the single zircon evaporation method, we used a conventional U-Pb method (Table 4, Fig. 6d). Each fraction consists of four to seven zircons of the same morphological features. Fractions 1-3, and 5 represent the first group and fraction 4 belongs to the second one (Table 4). Obtained ages do not form a reliable single discordia line (Fig. 6d). Calculated upper and lower intercept ages gave high errors and high a MSWD value. Three fractions lie near the concordia. The fraction 1 reveals U loss and gives U-Pb ages of 308 and 315 Ma which is in accordance with the magmatic ages obtained by the single zircon evaporation method. Fractions 3 and 5 yield U-Pb ages of 330/334 and 390/399 Ma, respectively. These ages are more concordant than the ages of the previous fraction. The age of the fraction 3 may have a geological meaning because some of the evaporated zircons have similar ages of 330-355 Ma. These ages may reflect a long time interval during which the hornblende- biotite granites were forming. We interpret the age of the fraction 5 (399 Ma) as the age of inherited zircons or as a mixed age of several zircons. Fractions 2 and 4 (Table 4) reflect inherited or mixed zircon ages. Following [31] we calculated forced regressions through 308 Ma to evaluate a possible age range of inherited zircons (Fig. 6d). This gives a range between 650 and 1300 Ma which is in accordance with the inherited zircon ages obtained by the single zircon evaporation method.

5.2.1.3. Leucocratic gneiss

The age of the leucocratic gneisses is poorly constrained because of fewer amounts of zircons. Only two grains have been extracted from the sample Gk39 (see Fig. 1 for location). The grain 1 (Table 5) gave 313.3±10 Ma in the first heating step and older (~350 Ma) ages at higher evaporation temperatures. The grain 2 yielded only old ages more than 650 Ma (Table 5). Taking the geological relationships into account we infer that 313±10 Ma is a magmatic age of the leucocratic orthogneisses. The scatter of older inherited or mixed ages in the sample Gk 39 is similar to the scatter in hornblende-biotite and biotite-muscovite orthogneisses. This feature makes the leucocratic gneisses different from the Kırklareli granites.

5.2.2. Permian granitoids

The Kırklareli granites have already been dated by Aydın [1, 10] and Okay *et al.* [2] as 245 Ma and ~271 Ma accordingly. In this study we have obtained ages intermediate between these

Table 5. Ages of leucocratic gneisses derived from single grain evaporation method. Errors are two-sigma standard deviations (2σ).

Sample/Grain	Evaporation temperature C	No. of scans	Mean ratio of $^{207}Pb/^{206}Pb$/error	Age (Ma)	Error (Ma)
Gk 39					
grain1	1380	145	0.05349 ±39	313.3	10
grain1	1400	108	0.05264 ±23	349.6	17
grain1	1420	144	0.05359 ±25	353.9	11
grain2	1380	109	0.06125 ±41	648	14
grain2	1400	111	0.06747 ±24	852.3	7.3
grain2	1420	36	0.07351 ±60	1028	16

reported dates. Only one sample (Gk 18) has been used for single zircon evaporation method. This sample is an augen gneiss consisting of quartz, porphyroblasts of strongly altered and in places completely recrystallized K-feldspar, altered plagioclase, brown muscovite, epidote, sphene, and rutile.

Zircons of this sample form a uniform population represented by brown, semi-transparent, and euhedral, prismatic crystals. Cl images of selected grains are shown in Figure 5c. Clear oscillatory magmatic zoning is characteristic for all selected grains.

All evaporated grains yielded ages between 253.8 and 276.1 Ma (Table 6) which give weighted average mean of 257 ± 6.2 Ma (Fig. 6c) that is similar to Okay *et al*. [2] data. Neither ours nor Okay *et al*. [2] studies who used the same zircon evaporation technique have revealed a large scatter of ages typical for the presence of inherited zircon core. Interestingly, grains 1 and 2 show decrease of ages with the rise of the evaporation temperature.

6. Discussion

Geological mapping, structural and geochemical studies, and isotopic dating indicate that the Paleozoic history of the Strandja massif included Carboniferous and Permian episodes of magmatic activity. The Permian magmatic episode has been established by previous studies [1, 10, 12, 2] and confirmed by this study. The Carboniferous episode is described for the first time.

The Carboniferous hornblende-biotite, biotite-muscovite, and leucocratic orthogneisses yield approximately same ages of 312-314 Ma. These rocks have not been mapped in the previous studies [12, 2] therefore it is difficult to estimate their total volume in the basement of the Strandja massif. However, it is worth noting that in the studied area they constitute about 70 % of the basement thus indicating that deciphering their nature is crucial for the understanding of the tectonic history of the Strandja massif.

Geochemical data suggest the evolution of Carboniferous magmas followed a calc-alkaline trend starting with granitoids from which the hornblende-biotite orthogneisses were formed and ending with the granites that now occur as the leucocratic gneisses. Crosscutting relationships of the leucocratic gneisses with the hornblende-biotite and biotite-muscovite orthogneisses supports this inference however relationships between two later types are reworked by Mesozoic deformations. Relationships between major elements indicate similarity of the hornblende-biotite orthogneisses with metaluminous I-type granitoids. The abundance of mafic schlierens suggests repeated injections of mafic magmas into an evolving magmatic chamber. The biotite-muscovite orthogneisses reveal peraluminous features and intermediate character between I- and S- types of granitoids. Finally, the leucocratic orthogneisses exhibits peraluminous, and S-type character. Taken together all of these features suggest that Carboniferous magmatic rocks evolved within a mature magmatic arc.

The mature crust of the Carboniferous arc can be inferred from abundant inherited zircon ages that have been detected in all of the Carboniferous metamorphic rocks. Some magmatic zircons from these rocks reveal consistent ages at all heating steps suggesting that these zircons are xenocrysts inherited from previously emplaced magmatic rocks. Zircon ages between 320 and 370 Ma obtained in this study (Fig. 4 and 5, Table 2, 3, 4, and 5) are correlative with magmatic ages of granitoids in neighboring regions of Bulgaria [32, 5] and they correspond to ages of magmatic rocks that are known as early Variscan granitoids in Europe [33, 34]. The time interval between 420 and 600 Ma is also almost completely covered by our dates (Fig. 4). Similar ages (~450, 560, 665, and 975 Ma) of inherited zircons have been reported by Carrigan *et al*. [35] in the Balkan tectonic unit of Bulgaria. These correlations suggest that inherited or mixed ages obtained in this study indicate a long-lived magmatic activity within the Strandja massif. The long-lived magmatic activity is a characteristic feature of the arc tectonic setting.

Major elements ratios show that the Kırklareli metagranites are of I-type being transitional between metaluminous and peraluminous granitoids (Fig. 2 and 3, Table 1). Similar to the Carboniferous orthogneisses the Kırklareli metagranites show the calc-alkaline trend of differentiation (Fig. 3). These geochemical features are not too decisive for an interpretation of a possible tectonic setting. Considering

Table 6. Ages of Kırklareli metagranites derived from single grain evaporation method. Errors are two-sigma standard deviations (2σ)

Sample/Grain	Evaporation temperature C	No. of Scans	Mean ratio of $^{207}Pb/^{206}Pb$/error	Age (Ma)	Error (Ma)
Gk18					
grain1	1370	144	0.05130±28	254.3	7.9
grain1	1390	142	0.051272±44	253.8	2.1
gran2	1380	106	0.05179±19	276.1	8.2
grain2	1400	107	0.051503±98	263.4	4.4
grain3	1380	73	0.05179±15	276.1	6.6
grain4	1380	146	0.0513±11	254.3	5.1
grain4	1400	142	0.051202±85	259.9	3.9
grain4	1420	142	0.051494±99	263	4.4

tectonic evolution of Tethysides, Şengör *et al*. [13] interpret the Permian and Triassic magmatism of the Strandja massif as subduction related. Taking into consideration correlations with the Variscan belt Okay *et al*. [2] infer a post-collisional setting of the Kırklareli granites.

Okay *et al*. [2] also suggest the anatectic nature of these granites. We disagree with this conclusion for following reasons. 1) Migmatization relevant to the Kırklareli pluton occurs only along the southern margin of the intrusion where amount of migmatites rarely exceeds 10 % of total volume of country rocks. 2) Xenoliths of country rocks were observed only at margins of the pluton but they are absent in its internal parts. 3) The composition of the pluton is very homogenous suggesting that it represents a single magmatic phase.

In accord with this observation we want to add that all studied zircons in the Kırklareli metagranite (Table 6) reveal no inherited or mixed ages. Zircons studied by Okay *et al*. [2] both in Kırklareli and other plutons of this type have the same character. At the same time, crosscutting relationships of the Kırklareli pluton with the country rocks are obvious from the geological map (Fig. 1). We infer that the formation of the Kırklareli magmas was due to influx of the high temperature mantle magmas to the base of the crust where it was contaminated with crustal components or facilitate generation of crustal melt at elevated temperatures that remelted earlier formed zircons. The following emplacement of such magmas to high crustal levels caused the formation of the Kırklareli type plutons in the Strandja massif. The mechanism outlined is more suitable for subduction related tectonic setting. The presence of oceanic and arc related rocks within a Strandja type of Triassic in Bulgaria, in which a stratigraphic conformity with Paleozoic rocks is admitted, is another argument in favor of this inference [3, 17, 36, 13].

There is abundant literature on tectonic settings of the granitoids, their ages, and the timing of metamorphism in the Variscan belt of Europe [33-35, 37-47]. Magmatic activity there [25, 35, 40, 48-63] occurred over a time interval (320 to 290 Ma) which is similar to those in the Strandja massif. Taking into consideration S-type of intrusions the majority of researches assigned them to post-collisional tectonic settings. However, some researchers consider a possibility of subduction-related tectonic setting pointing to the presence of calc-alkaline character of some intrusions and their definite I-type (.e.g [51]) for magmatic rocks of 310 Ma in Bulgaria). Moreover, Matte [64] infers that during the Westphalian time (~318-303 Ma) the western part Variscan belt was characterized by the Himalayan-type mountain building while its eastern part was still represented by an Andean-type of active margins. Typical I-type granitoids in Variscan belt, their isotopic composition and REE abundances show either continental contribution to mantle derived magmas or remelting of lower continental crust. Some differentiation diagrams have been proposed to determine the tectonic settings of granitoids [65] but generally our samples fall to the junction subduction-related and syn-collisional granites [16]. This matter was discussed in detail by Förster *et al*. [66].

This correlation indicates that more work needs to be done for the solution of the first order questions concerning tectonic setting of the Carboniferous and Permian magmatism both in Strandja massif and surrounding regions.

7. Conclusions

The Pb/Pb zircon evaporation studies of the orthogneisses constituting the Paleozoic basement of the Strandja massif have revealed a voluminous Carboniferous magmatic episode at 310 to 320 Ma. After an episode of metamorphism and deformation it was followed by emplacement of the early Permian (257±6 Ma) monzogranites of the Kırklareli type.

The Carboniferous magmatic rocks have geochemical features that allow considering them as subduction related. Ages of inherited magmatic zircons indicate a long lived magmatic activity within the Strandja massive that collaborate the inference about subduction nature of the medial Paleozoic magmatism. It also testifies that the basement of the arc was continental and included Precambrian protoliths.

The Permian magmatic rocks belong to calc-alkaline series but in contrast to the Carboniferous they have a narrower compositional range and on discrimination diagrams are located close the metaluminous/peraluminous boundary. Tectonic setting of these rocks in conjunction with geochemical features also allows interpreting them as subduction related.

Acknowledgements

This study was supported by TÜBITAK (The Scientific and Technical Research Council of Turkey, Project no: YDABCAG 101Y010) and resulted from the cooperative study between Istanbul Technical University, Turkey and University of Tübingen, Germany. G. Bartholomä and H. Taubald for the XRF analysis are gratefully acknowledged. We wish to thank W. Siebel and E. Reitter for help in isotopic measurements. We warmly thank T.T.B. Nuguyen for help in mineral separation and isotopic measurements. We sincerely thank G. Topuz for constructive comments on geochemistry part, and O. Vonderschmidt and A. Dikbaş for valuable assists in the field study. We also thank Prof. Aral Okay for his extensive comments on an earlier version of this paper that significantly improved it.

References

[1] Aydın Y., Etude petrographique et geochimique de la partie centrale du Massif d'Istranca (Turquie), Thesis, University of Nancy (1974).

[2 Okay A.I., Satır M., Tüysüz O., Akyüz S., Fukun C., The tectonics of the Strandja Massif: late-Variscan and mid-Mesozoic deformation and metamorphism in the Northern Aegean. Int. J. Earth Sciences 90 (2) (2001) 217-233.

[3] Chatalov G., Recent developments in the geology of the Strandja Zone in Bulgaria. Bull. Tech. Univ. Istanbul 41 (1988) 433-466.

[4] Haydoutov I., Yanev S., The Protomoesian microcontinent of the Balkan Peninsula – a peri-Gondwanaland piece. Tectonophysics 272 (1997) 303-313.

[5] Yanev S., Palaeozoic terranes of the Balkan Peninsula in the framework of Pangea assembly. Palaeogeography, Palaeoclimatology, Palaeoecology 161 (2000) 151-177.

[6] Ketin İ., Anadolu'nun tektonik birlikleri. M.T.A. Derg. 66 (1966) 75-88.

[7] Şengör A.M.C., Yılmaz Y., Tethyan evolution of Turkey: A plate tectonic approach. Teconophysics 75 (1981) 181-241.

[8] Okay A.I., Satir M.. Maluski H., Siyako M., Monie P., Metzger R., Akyüz S. Paleo- and Neo-Tethyan events in northwestern Turkey: geologic and geochronologic constraints. In: A. Yin and M. Harrison (Editors), The Tectonic Evolution of Asia. Rubey Colloquium. Cambridge University Press, Cambridge, 1996, pp. 420-441.

[9] Okay A.I., Tüysüz O., Tethyan sutures of northern Turkey. In: B. Durand, L. Jolivet, F. Horvath and M. Seranne (Editors), The Mediterranean Basins: Tertiary Extension within the Alpine Orogen. Geological Society, London, Special Publication, 156, 1999, pp. 475-515.

[10] Aydın Y., Geology of the Yıldız (Istranca) Mountains. Thesis, Istanbul Technical University, İstanbul, 1982, 106 p.

[11] Yılmaz Y., Tüysüz O., Yiğitbas E., Genç Ş.C., Şengör A.M.C., Geology and tectonic evolution of the Pontides. In: A.G. Robinson (Editor), Regional and Petroleum geology of the Black Sea and surrounding region. AAPG Memoir 68, 1997, pp. 183-226.

[12] Çağlayan A.M., Şengün M., Yurtsever A., Main fault systems shaping the Istranca Massif, Turkey, J. Pure Appl. Sci. Ser. A Geosci. 21 (1988) 145-154.

[13] Şengör A.M.C., Yılmaz Y., Sungurlu O., Tectonics of the Mediterranean Cimmerides: Nature and evolution of the western termination of Paleo-Tethys. In: J.E. Dixon and A.H.F. Robinson (Editors), The geological evolution of the Eastern Mediterranean. Geological Society of London Special Publication 17, 1984, pp. 77-112.

[14] Türkcan A., Yurtsever A., Geological map of Turkey. Istanbul. General Derectorate of Mineral Researc and Exploration (2002), Ankara.

[15] Natal'in B.A., Sunal G., Toraman E., Dextral arc-parallel tectonic transport along the southern margin of Eurasian in the late Paleozoic-early Mesozoic, 1st International Symposium of Istanbul Technical University the Faculty of Mines on Earth Sciences and Engineering 16-18 May, 2002, Istanbul Technical University (ITU) (2002) 80.

[16] Natal'in B. A., Satir M., Sunal G., Toraman E., Structural and metamorphic evolution of the Strandja massif. Final report of the 101Y010 Project, Türkiye Bilimsel Teknik Araştırma Kurumu, Yer Deniz Atmosfer Bilimleri ve Çevre Araştırma Grubu Ankara, 2005.

[17] Chatalov G.A., Triassic in Bulgaria - A review. Bulletin of the Technical University of Istanbul 44(1-2) (1991)103-135.

[18] Paterson S.R., Pignotta G.S., Vernon R.H., The significance of microgranitoid enclave shapes and orientations. Journal of Structural Geology, 26(8) (2004)1465-1481.

[19] Wiebe R.A., Collins W.J., Depositional features and stratigraphic sections in granitic plutons: implications for the emplacement and crystallization of granitic magma. Journal of Structural Geology 20(9-10) (1998) 1273-1289.

[20] Vernon R.H., Review of Microstructural Evidence of Magmatic and Solid-State Flow. Electronic Geosciences 5 (2000).

[21] Kober B., Whole-grain evaporation for 207Pb/206Pb age investigations on single zircons using a double-filament thermal ion source. Contrib. Mineral. Petrol. 93 (1986) 481-490.

[22] Kober B., Single-zircon evaporation combined with Pb+ emitter-bedding for 207Pb/206Pb-age investigations using thermal ion mass spectrometry, and implications to zirconology. Contrib. Mineral. Petrol. 96 (1987) 63-71.

[23] Stacey J.S., Kramers J.D., Approximation of terrestrial lead isotope evolution by a two stage model. Earth Planet. Sci. Lett. 26 (1975) 207-221.

[24] Chen F., Siebel W., Satır M., Terzioğlu N., Saka K., Late Proterozoic continental accretion in the north-western Turkey: evidence from zircon U–Pb and Pb–Pb dating and Nd–Sr isotopes. Int. J. Earth Sci. 91 (2002) 469-481.

[25] Siebel W, Chen F., Satır M., Late-Variscan magmatism revisited: new

implications from Pb-evaporation zircon ages on the emplacement of redwitzites and granites in NE Bavaria, International Journal of Earth Sciences 92 (2003) 36-53.

[26] Siebel W., Inferences about magma mixing and thermal events from isotopic variations in redwitzites near the KTB site. KTB Rep 94(3) (1994) 157-164.

[27] Nguyen T.T.B., Satır M., Siebel W., Chen F., Granitoids in the Dalat zone, southern Vietnam: age constraints on magmatism and regional geological implications, Int. J. Earth Sci. (Geol Rundsch), 93 (2004) 329-340.

[28] Le Maitre R.W., A classification of ingeous rocks and glossary of terms. Blackwell, Oxford, 1989,193 p.

[29] O'Connor J.T., A classification for quartz-rich igneous rocks based on feldspar ratios. US Geol. Surv. Prof. Pap. B525 (1965) 79-84.

[30] Nemchin A.A., Pidgeon R.T., Evolution of the Darling Range Batholith, Yilgarn Craton, Western Australia: a SHRIMP zircon study. J. Petrol. 38 (1997) 625-649.

[31] Chen F., Todt W., Hann H. P., Zircon and garnet geochronology of eclogites from the Moldanubian Zone of the Black Forest, Germany, The Journal of Geology 111 (2003) 207-222.

[32] Zagorchev I.S., Rhodope controversies. Episodes 21(3) (1998)159-166.

[33] Finger F., Roberts M.P., Haunschmid B., Schermaier A., Steyrer H.P., Variscan granitoids of central Europe: their typology, potential sources and tectonothermal relations. Mineral. Petrol., 61 (1997) 67-96.

[34] Klötzli U.S., Koller F., Scharbert S., Höck V., Cadomian lower-crustal contributions to Variscan granite petrogenesis (South Bohemian pluton, Austria): Constraints from zircon typology and geochronology, whole-rock, and feldspar Pb-Sr isotope systematics. J. Petrol. 42 (2001) 1621-1642.

[35] Carrigan C.W., Mukasa S.B., Haydoutov I., Kolcheva K., Age of Variscan magmatism from the Balkan sector of the orogen. Lithos 82 (2005) 125-147.

[36] Şengör A.M.C., The Cimmeride orogenic system and the tectonics of Eurasia. The Geological Society of America, Special Paper 195, 1984, 82 p.

[37] O'Brien P.J., Carswell D.A., Gebauer D., Eclogite formation and distribution in the European Variscides. In: D.A. Carswell, Editor, Eclogite Facies Rocks, Blackie, Glasgow, 1990, pp. 204-224.

[38] Kalt A., Hanel M., Schleicher H., Kramm U., Petrology and geochronology of eclogites from the Variscan Schwarzwald (F.R.G.). Contrib Mineral. Petrol. 115 (1994) 287–302.

[39] Kalt A., Corfu F., Wijbrans J.R., Time calibration of a P–T path from a Variscan high-temperature low-pressure metamorphic complex (Bayerischer Wald, Germany), and the detection of inherited monazite. Contrib. Mineral. Petrol. 138 (2000) 143–163.

[40] Kröner A., Hegner E., Hammer J., Haase G., Bielicki K.H., Krauss M., Eidam J., Geochronology and Nd-Sr systematics of Lusatian granitoids: significance for the evolution of the Variscan orogen in east-central Europe. Geol. Rundsch. (Int. J. Earth Sci.) 83 (1994) 357-376.

[41] Kröner A., O'Brien P.J., Nemchin A.A., Pidgeon R.T., Zircon ages for highpressure granulites from South Bohemia, Czech Republic, and their connection to the Carboniferous high temperature processes. Contrib. Mineral. Petrol. 138 (2000) 127-142.

[42] Schaltegger U., Magma pulses in the Central Variscan Belt: episodic melt generation and emplacement during lithospheric thinning. Terra Nova 9 (1997) 242-245.

[43] Schaltegger U., U-Pb geochronology of the Southern Black Forest Batholith (Central Variscan Belt): timing of exhumation and granite emplacement. Int. J. Earth Sci. 88 (2000) 814-828.

[44] Fernández-Suárez J., Dunning G.R., Jenner G.A., Gutiérrez-Alonso G., Variscan collisional magmatism and deformation in NW Iberia: constraints from U-Pb geochronology of granitoids. J. Geol. Soc. London, 157 (2000) 565-576.

[45] von Raumer J.F., The Palaeozoic evolution in the Alps: from Gondwana to Pangea, Geol Rundsch, 87 (1998) 407–435.

[46] Friedl G., Finger F., Paquette J.L., von Quadt A., McNaughton N.J., Fletcher I.R., Pre-Variscan geological events in the Austrian part of the Bohemian Massif deduced from U–Pb zircon ages, Int. J. Earth Sci. (Geol Rundsch) 93 (2004) 802–823.

[47] Romer R.L., Rötzler J., P-T-t evalution of ultrahigh-temperature granulites from the Saxon Granulite Massif, Germany. Part II: Geochronology. Jornal of Petrology 42 (2001) 2015-2032.

[48] Peytcheva I., von Quadt A., U-Pb zircon dating of metagranites from Byala-reka region in the east Rhodopes, Bulgaria. Proceedings of the XV Congress of the Carpatho- Balcan Geological Association, Sept., 1995, Athens, Geol. Soc. Greece Special Publication, 4(2) (1995) 637-642.

[49] Peytcheva I., Salnikova E., Kostitsyn Yu., Ovtcharova M., Sarov S., Metagranites from the Madan- Davidkovo dome, Central Rhodopes: U-Pb and Sr-Rb protholite and metamorphism dating. ABCD-GEODE (2000) 67.

[50] Cherneva Z., Ovtcharova M., von Quadt A., Kolcheva K., Stancheva E., Sarov S., Peytcheva I., Monazite and zircon U-Pb ages of migmatites from the Arda River Valley, Central Rhodopian Dome, Bulgaria. Proc. Annual Scientific Conference of BGS, Sofia. (2002) 20-22.

[51] Carrigan C.W., Mukasa S.B., Haydoutov I., Kolcheva K., Ion microprobe U-Pb zircon ages of pre-Alpine rocks in the Balkan, Sredna Gora, and Rhodope terranes of Bulgaira: Constraints on Neoproterozoic and Variscan tectonic evolution. J. Czech Geol. Soc., 48 (2003) 32-33.

[52] Gerdes A., Friedl G., Parrish R.R., Finger F., High-resolution geochronology of Variscan granite emplacement – the South Bohemian Batholith. J. Czech Geol. Soc., 48 (2003) 53-54.

[53] Azevedo M.R., Valle Aguado B., Schaltegger U., Nolan J., Medina J., Martins M.E., U-Pb zircon and monazite geochronology of Variscan magmatism related to synconvergence extension in central northern Portugal. J. Czech Geological Soc. 48 (2003), 16.

[54] Schaltegger U., Corfu F., The age and source of late Hercynian magmatism in the central Alps: evidence from precise U-Pb ages and initial Hf isotopes. Contrib. Mineral. Petrol. 111 (1992) 329-344.

[55] von Quadt A., Grünenfelder M. and Büchi H., U-Pb zircon ages from igneous rocks of the Bernina nappe system (Grisons, Switzerland). Schweiz. Mineral. Petrogr. Mitt., 74 (1994) 373-382.

[56] Siebel W., Constraints on Variscan granite emplacement in northeast Bavaria, Germany: further clues from a petrogenetic study of the Mitterteich granite. Geol. Rundsch 84 (1995) 384–398.

[57] Siebel W., Trzebski R., Stettner G., Hecht L., Casten U., Höhndorf A., Müller P., Granitoid magmatism of the NW Bohemian massif revealed: Gravity data, composition, age relations and phase concept. Geol. Rundsch. 86(suppl) (1997) 45–63.

[58] Cocherie A., Guerrot C., Rossi P.H., Single-zircon dating by stepwise Pb evaporation: comparison with other geochronological techniques applied to the Hercynian granites of Corsica, France. Chem. Geol. 101 (1992) 131-141.

[59] Schmidberger S.S., Hegner E., Geochemistry and isotope systematics of calc-alkaline volcanic rocks from the Saar-Nahe basin (SW Germany) - implications for Late-Variscan orogenic development, Contrib. Mineral. Petrol. 135 (1999) 373-385.

[60] Amov B., Arnaudov V., Lead isotope data on the Paleozoic granitoids and ore mineralization from western Balkan and Tran district. I. Isotope and geochronology. Geol. Balc. (1981) 11-2.

[61] Kamenov B., von Quadt A., Peytcheva I., New insight into petrology, geochemistry, and dating of the Vejen pluton, Bulgaria. Geochemistry, Mineralogy, and Petrology 39 (2002) 3-26.

[62] Peytcheva I., von Quadt A., Ovtcharova M., Handler R., Neubauer F., Salnikova E., Kostitsyn Y., Sarov S., Kolcheva K., Metagranitoids from the eastern part of the Central Rhodopean Dome (Bulgaria): U–Pb, Rb–Sr and 40Ar/39Ar timing of emplacement and exhumation and isotope-geochemical features, Mineralogy and Petrology 82 (2004) 1-32.

[63] Bonin B., Orogenic to non-orogenic magmatic events: overview of the late Variscan magmatic evolution of the Alpine Belt. Turkish Journal of Earth Sciences, 7 (1998) 133-143.

[64] Matte P., Variscides between the Appalachians and the Urals: similarities and differences between Paleozoic subduction and collision belts. Spec. Pap. Geol. Soc. Am. 364 (2002) 239– 251.

[65] Pearce J.A., Harris N.B.W., Tindle A.G., Trace element discrimination diagrams for the tectonic interpretation of granitic rocks. J. Petrol. 25 (1984) 956-983.

[66] Förster H.J., Tischendorf G., Trumbull R.B., An evaluation of the Rb vs. (Y + Nb) discrimination diagram to infer tectonic setting of silicic igneous rocks, Lithos, 40 (1997) 261-293.

[67] Maniar P.D., Piccoli P.M., Tectonic discrimination of granitoids. Bulletin of the American Geological Society 101 (1989) 635–643.

[68] Shand S.J., Eruptive Rocks, D. Van Nostrand Company, New York, 1927, pp. 360.

[69] Irvine T.N., Barager W.R.A., A guide to the chemical classification of the common volcanic rocks, Canadian Journal of Earth Sciences 8 (1971) 523-548.

[70] Ludwig K.R., Isoplot 3.0, A Geochronological Toolkit for Microsoft Excel, Berkeley Geochronology Center Special Publication, 2003, No. 4.